Neuron, Vol. 28, 941–953, December, 2000, Copyright ©2000 by Cell Press

Size of Vesicle Pools, Rates of Mobilization, and Recycling at Neuromuscular Synapses of a *Drosophila* mutant, *shibire*

Ricardo Delgado,*‖ Carlos Maureira,*†‖ Carolina Oliva,*‖ Yoshiaki Kidokoro,‡ and Pedro Labarca*§
*Centro de Estudios Cientificos
Arturo Prat 514
Valdivia
Chile
†Escuela de Postgrado
Fac. de Ciencias
Universidad de Chile
‡Gunma University School of Medicine
3-39-22 Showa-machi
Maebashi 371-8511
Japan

Summary

Two vesicle pools, readily releasable (RRP) and reserve (RP) pools, are present at *Drosophila* neuromuscular junctions. Using a temperature-sensitive mutant, *shibire*^{ts}, we studied pool sizes and vesicle mobilization rates. In *shibire*^{ts}, due to lack of endocytosis at nonpermissive temperatures, synaptic currents continuously declined during tetanic stimulation until they ceased as the result of vesicle depletion. By then, ~84,000 quanta were released. Vesicles were mobilized from RP at a rate 1/7–1/10 of RRP. Cytochalasin D inhibited mobilization of vesicles from RP, allowing us to estimate the size of RRP as 14%–19% of all vesicles. Vesicle recycling supports synaptic transmission during prolonged tetanic stimulation and the maximum recycling rate was 1000 vesicles/s.

Introduction

Vesicle availability and dynamics are essential for synaptic transmission during sustained nerve activity and for synaptic plasticity both at peripheral and central synapses and in neuroendocrine cells (Neher and Zucker, 1993; Ryan and Smith, 1995; De Camilli and Takei, 1996; Zucker, 1996; Smith et al., 1998; Stevens and Wesseling, 1998). Synaptic vesicles are recycled after release of transmitter (Heuser and Reese, 1973). Two pathways for vesicle recycling were documented in *Drosophila* synapses (Koenig and Ikeda, 1996). The process of vesicle recycling is conveniently studied by the use of fluorescent dyes (Betz and Bewick, 1992). Using a dye, FM1-43, Kuromi and Kidokoro (1998, 1999, 2000) identified two pools of synaptic vesicles, exo/endo cycling (readily releasable pool, RRP) and reserve pools (RP), at the larval *Drosophila* neuromuscular junction. The RRP is located in the periphery of each presynaptic bouton, whereas RP is in the center. During short periods of neuronal activity or low-frequency nerve stimulation (1–3 Hz), synaptic vesicles in RRP, but not those in RP, participate in transmitter release. During intense neuronal activity or high-frequency nerve stimulation (>10 Hz), vesicles in RP are recruited.

To understand vesicle dynamics in the presynaptic terminal during sustained neuronal activity, we asked the following questions: what is the size of vesicle pools? What is the rate of vesicle mobilization from these pools? And to what extent vesicle recycling is contributing in maintaining synaptic transmission during prolonged tetanic stimulation? Combining measurements of nerve-evoked synaptic currents and imaging of FM1-43 in synaptic boutons, these questions can be answered by taking advantage of a temperature-sensitive paralytic mutant, *shibire*^{ts} (*shi*^{ts}). In *shi*^{ts} endocytosis ceases and synaptic vesicles are completely depleted after synaptic activation at nonpermissive temperatures, while synaptic transmission at room temperature is normal (Koenig and Ikeda, 1989, 1996; Koenig et al., 1989; Estes et al., 1996). This mutant provides a means to estimate the size of vesicle pools and their rates of mobilization at the larval neuromuscular junction. The contribution of recycling for synaptic transmission can be examined in wild-type larvae at steady state during repetitive nerve stimulation.

The total number of vesicles in *shi*^{ts} can be measured directly by counting the number of quanta released at nonpermissive temperature. To estimate the size of two pools separately, we need to inhibit recruitment of vesicles from RP. Kuromi and Kidokoro (1998) reported in *shi*^{ts} that cytochalasin D (cyt-D), which blocks actin polymerization (Cooper, 1987), inhibits labeling of vesicles in the reforming RP at room temperature after complete depletion at nonpermissive temperature. However, it is not known whether cyt-D prevents mobilization of vesicles already stored in RP. If it does, then the size of RRP can be measured in *shi*^{ts} at nonpermissive temperature after cyt-D treatment. This study has been partly published in the abstract form (Delgado et al., 2000, J. Physiol., abstract).

Results

Synaptic Transmission at Room Temperature

Synaptic currents evoked by tetanic nerve stimulation at 10 Hz were studied first at room temperature (19°C–23°C). Upon tetanic nerve stimulation, evoked currents declined quickly during initial few stimuli, slowly during subsequent 50 s, and finally reached a steady state (Figure 1A, top panels marked *CS* and *shi*^{ts1}). The initial amplitude of evoked currents was 378 ± 32 nA (n = 11) in *CS* and 382 ± 50 nA (n = 11) in *shi*^{ts1} (mean ± SEM; n, number of cells). At the steady state, mean current amplitudes were 176 ± 24 nA (n = 11) in *CS* and 140 ± 22 nA (n = 11) in *shi*^{ts1}. Initial amplitude and steady-state current amplitudes were indistinguishable between *CS* and *shi*^{ts1} at all frequencies tested ($p > 0.05$).

The decline in evoked current amplitudes could reflect postsynaptic receptor desensitization due to L-gluta-

§To whom correspondence should be addressed (e-mail: plabarca@cecs.cl).
‖These authors contributed equally to this study.

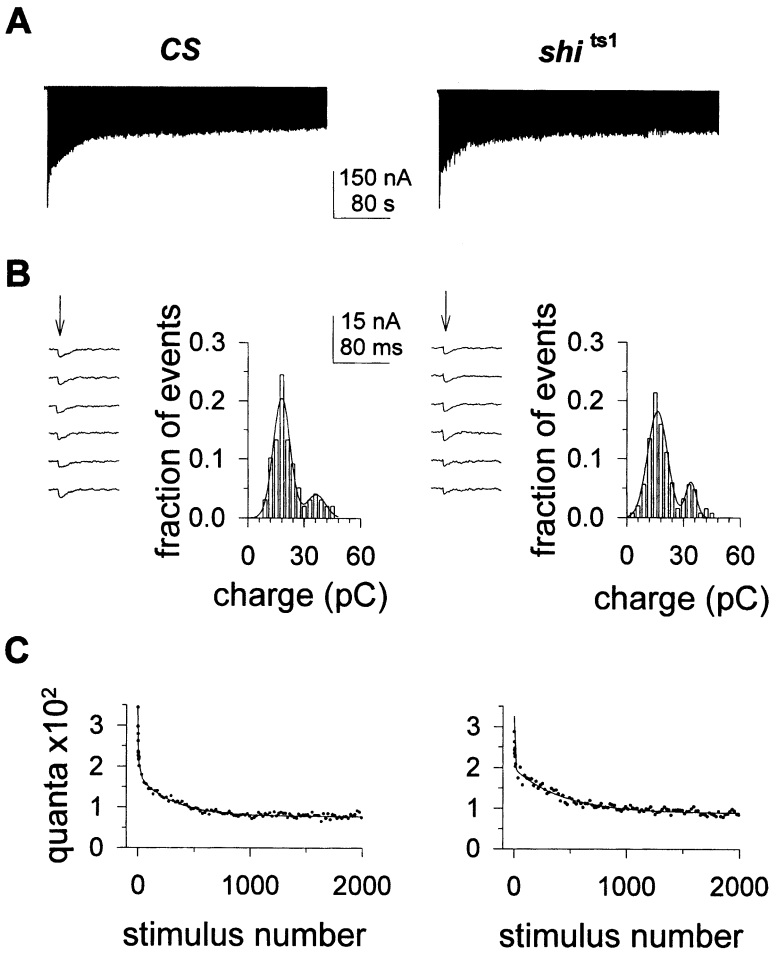

Figure 1. Synaptic Transmission at Room Temperature

(A) Nerve-evoked synaptic currents in *CS* (left panel) and *shi*^{ts1} (right panel) during tetanic nerve stimulation at 10 Hz for 400 s at room temperature.

(B) Nerve-evoked synaptic currents in 75 μM external Ca^{2+} in *CS* (left panels) and *shi*^{ts1} (right panels). In this condition, the failure rate was >0.7, and a majority of evoked synaptic currents were unitary. Current traces were selected from records in which synaptic currents were evoked. Downward arrows indicate timing of nerve stimulation. The histograms display the distribution of synaptic current integrals in *CS* (left) and *shi*^{ts1} (right), from which unitary charge transfer was estimated. The solid lines are the best fit of two Gaussians.

(C) Number of quanta released by each stimulus is plotted against stimulus number. Graphs were constructed using the data shown in (A). The solid lines are best fit of the following function to the data:

$$Q_T = Q_1 \exp(-T/\tau_1) + Q_2 \exp(-T/\tau_2) + Q_\infty$$

Q_T is the quantal content at the T'th stimulus, Q_∞ is the quantal content at the steady state, Q_1 and Q_2 are constants in quantum, T is the stimulus number, and τ's are decay time constants in the unit of stimulus. For the experiments shown, fitting parameters were as follows—for *CS*, Q_1 = 139 quanta, τ_1 = 6.4 stimuli, Q_2 = 103 quanta, τ_2 = 284 stimuli, Q_∞ = 79 quanta; and for *shi*^{ts1}, Q_1 = 128 quanta, τ_1 = 4.7 stimuli, Q_2 = 110 quanta, τ_2 = 410 stimuli, Q_∞ = 90 quanta. Average decay constants obtained from fitting were as follows—for *CS*, $\tau_1 = 8.7 \pm 2.7$ stimuli, $\tau_2 = 320 \pm 29$ stimuli (n = 11); and for *shi*^{ts1}, $\tau_1 = 5.3 \pm 0.3$ stimuli, $\tau_2 = 315 \pm 45$ stimuli (n = 11). These parameters do not differ significantly between *CS* and *shi*^{ts1} ($p > 0.05$).

mate released in response to tetanic stimulation. Exposure to L-glutamate for an extended period of time reduces the amplitude and prolongs the time course of evoked synaptic potentials (Jan and Jan, 1976). We confirmed that prolonged exposure to L-glutamate (>400 μM) decreased the amplitude and slowed the time course of evoked synaptic currents. However, the time course of synaptic current amplitude decline during tetanus did not change in the presence of exogenous L-glutamate. Furthermore, the time course of individual synaptic currents at the steady state was not slower compared with earlier ones during tetanus (Figure 3B). Therefore, we concluded that the decline in amplitude during tetanus is not due to desensitization of postsynaptic glutamate receptors.

To estimate the quantal content of nerve-evoked synaptic currents, we used the amount of charge transferred during synaptic currents, instead of the amplitude, because the time course of nerve-evoked synaptic currents was not necessarily the same as that of unitary currents, probably due to slightly asynchronous release of each quantum. To measure charge transfer during unitary synaptic currents, evoked synaptic currents were recorded in *CS* and *shi*^{ts} in the external solution containing 75 μM Ca^{2+} in which the probability of release was low (failure rate > 0.7). Evoked synaptic currents recorded under such experimental conditions at room temperature had the mean amplitude of 1.6 ± 0.1 nA (n = 4) in *CS* and 1.7 ± 0.2 nA (n = 4) in *shi*^{ts1} and the decay time constant of 9.8 ± 0.4 ms (n = 4) in *CS* and 10.2 ± 1.0 ms (n = 4) in *shi*^{ts1}. Sample current traces are shown in Figure 1B (traces depicted in left panels for *CS* and *shi*^{ts1}). These values are similar to the amplitude of miniature synaptic currents (Zhong and Wu, 1991) and unitary evoked synaptic currents obtained under similar experimental conditions (Acharya et al., 1998). To estimate the charge transferred during unitary synaptic currents, these synaptic current traces were integrated, and the frequency histograms were constructed (Figure 1B, right panels for *CS* and *shi*^{ts1}). Two Gaussians were fitted to the histograms (solid lines). In the examples shown in Figure 1B, major peaks located at 16.9 pC in *CS* and 16.2 pC in *shi*^{ts1}, and minor peaks were at 33 pC for *CS* and 31 pC in *shi*^{ts1}. In both strains, the current integral at the minor peak is approximately twice of that at the major peak, suggesting that the major peak is due to release of one quantum and the minor one is due to synchronized release of two quanta. In population of cells, the major peaks at 16.1 ± 0.9 pC (n = 4) in *CS* and 16.3 ± 0.7 pC (n = 4) in *shi*^{ts1} were

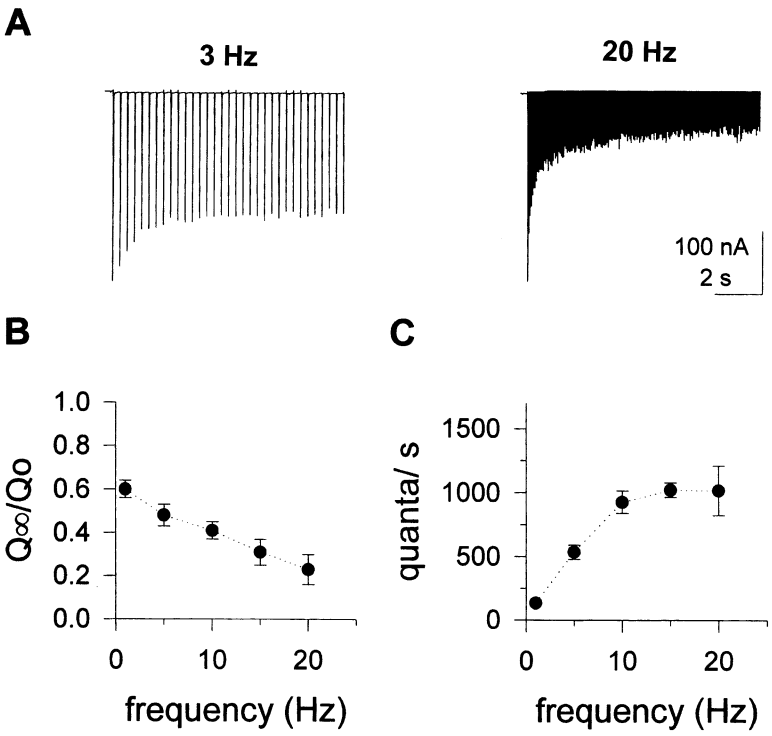

Figure 2. Effects of Stimulus Frequency on the Steady State of Transmitter Release

(A) Synaptic currents evoked by stimulus frequency of 3 Hz (left panel) and 20 Hz (right panel) at the same *CS* neuromuscular junction at room temperature.

(B) The ratio Q_∞/Q_0 is plotted against stimulus frequency, where Q_∞ is the quantal content at the steady state and Q_0 is that at the first stimulus.

(C) Plot of the rate of quantal release at the steady state against stimulus frequency. For (B) and (C) the bar attached to each symbol is SEM (n = 4).

taken as the amount of charge transferred during release of one quantum.

Quantal contents as a function of consecutive 10 Hz stimulation for the experiments in Figure 1A are shown in Figure 1C. The initial quantal content was 284 ± 32 quanta (n = 11) in *CS* and 277 ± 43 quanta (n = 11) in *shi*^{ts1}. The rate of release at the steady state was 101 ± 9 quanta/stimulus for *CS* and 88 ± 13 quanta/stimulus for *shi*^{ts1}, and the total quanta released during 200 s of repetitive stimulation at 10 Hz was 2.3 ± 0.1 × 10^5 (n = 11) for *CS* and 2.1 ± 0.3 × 10^5 (n = 11) for *shi*^{ts1}. Thus, at room temperature, synaptic properties in *CS* and *shi*^{ts1} were indistinguishable.

The time course of decline in the quantal content during tetanic stimulation was well fitted with two exponentials and a steady component (solid line in Figure 1C). The overall contribution of the fast component to transmitter release is small compared with that of the slow and steady components. The fast component was observed in all conditions examined in this study and may represent vesicles docked and primed at release sites. We term it the immediately releasable pool (IRP).

Estimation of Maximal Recycling Rates

If we assume that the steady state of synaptic current amplitude during tetanic stimulation continues indefinitely, the steady-state rate of quanta released per stimulus must equal the number of vesicles recycled. Thus, we examined the steady-state rate of transmitter release within the range between 1 and 20 Hz to investigate the effect of stimulus frequency on recycling rates. Currents evoked by nerve stimulation at 3 and 20 Hz at the same neuromuscular junction are depicted in Figure 2A. The initial decline of quantal content was fast and was observed at 3 Hz (Figure 2A) or even at 1 Hz (data not shown). Moreover, at all frequencies studied, the steady-state quantal content was significantly smaller relative to that at the first stimulus (Figure 2B). The steady-state rate of release increased up to 10 Hz to reach a maximum of ~1,000 quanta/s (Figure 2C), yielding an estimate of the maximal recycling rate under these experimental conditions.

Synaptic Transmission during Tetanic Nerve Stimulation at Nonpermissive Temperatures; Estimation of Total Number of Quanta

At nonpermissive temperatures the response to tetanic nerve stimulation in *shi*^{ts1} or in *shi*^{ts2} (Figure 3A, right panel) was remarkably different from that in *CS*. As depicted in Figure 3A (left panel), the temporal pattern of decline of synaptic current amplitudes in *CS* was similar to that at room temperature and, following a transient decline in current amplitude, a steady amplitude was achieved. Evoked synaptic currents in *CS* are depicted in Figure 3B in higher time resolution. In contrast, in *shi*^{ts1} at 32°C the steady state of transmitter release was never achieved, and the evoked current amplitude continuously declined until eventually transmitter release entirely ceased (Figure 3A, right panel, upper trace). Current records in *shi*^{ts1} at 32°C are shown in a higher time resolution in Figure 3B. The bottom trace was obtained at a higher gain, showing a complete absence of synaptic currents toward the end of tetanus. At 32°C unitary currents had larger amplitudes (2.3 ± 0.4 nA in *CS*, n = 4; 2.1 ± 0.1 nA in *shi*^{ts1}, n = 4), faster decay time constants (5.1 ± 0.4 ms in *CS*, n = 4; 5.9 ± 0.7 ms in *shi*^{ts1}, n = 4), and smaller amount of unitary charge transfer (13.7 ± 0.7 pC in *CS*, n = 4; 13.7 ± 0.5 pC in *shi*^{ts1}, n = 4) compared with those at room temperature. Initial current amplitudes in the standard external solu-

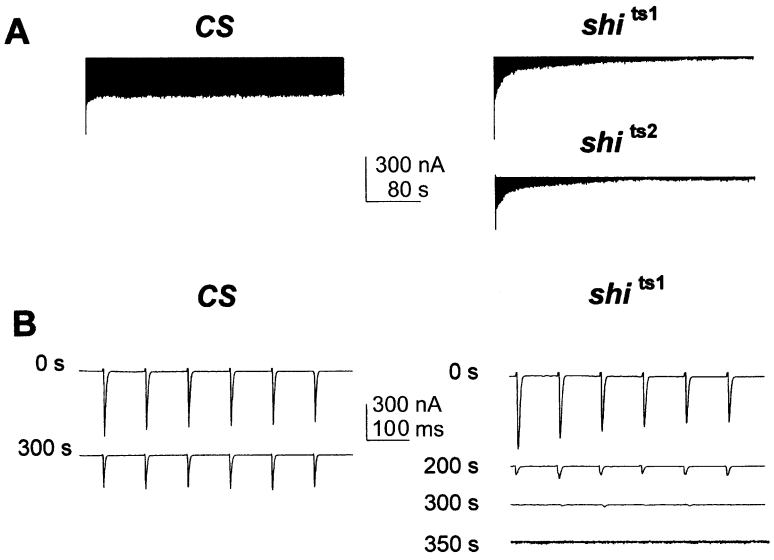

Figure 3. Decline of Synaptic Current Amplitudes during Prolonged 10 Hz Tetanic Stimulation at Nonpermissive Temperatures in *CS* and *shi*^{ts} Neuromuscular Junctions

(A) Decline of synaptic current amplitude during 400 s 10 Hz tetanic stimulation at 32°C in *CS* (left panel), *shi*^{ts1} (right panel, upper trace), and 34°C in *shi*^{ts2} (right panel, lower trace).

(B) Synaptic currents in higher time resolution in *CS* (left panel) and *shi*^{ts1} (right panel) recorded at the time indicated at the left of each trace after the onset of tetanic stimulation. The trace at 350 s in *shi*^{ts1} (bottom trace) was obtained at higher amplification (5×) showing a complete absence of synaptic currents after 3500 stimuli.

tion were larger at 32°C (522 ± 24 nA in *CS*, n = 6; 500 ± 77 nA in *shi*^{ts1}, n = 6) and had faster decay time constants. The total number of quanta released in *shi*^{ts1}, by the time when complete depletion was achieved at 10 Hz, averaged 8.3 ± 1.2 × 10^4 quanta (n = 6).

To test whether the characteristics of synaptic transmission in *shi*^{ts1} at nonpermissive temperature are specific to a mutation at the *shi* locus, we repeated the depletion experiment using another allele, *shi*^{ts2} (Figure 3A, right panel, lower trace). Experiments were performed at 34°C, at which temperature complete depletion of vesicles has been documented in EM (Estes et al., 1996). At 34°C, initial current amplitudes in *shi*^{ts2} were significantly smaller (230 ± 50 nA, n = 5) than in *shi*^{ts1} at 32°C. In contrast, within experimental error, unitary current amplitudes at 34°C in 75 μM external Ca^{2+} (3.4 ± 0.3 nA, n = 6 in *shi*^{ts1}; 2.9 ± 0.2 nA, n = 6 in *shi*^{ts2}) and unitary charge transfer (11.0 ± 1.0 pC, n = 6 in *shi*^{ts1}; 10.6 ± 1.3 pC, n = 6 in *shi*^{ts2}) were not different ($p > 0.05$) between these two alleles. Likewise, the decline of quantal content during depletion in *shi*^{ts2}, as in *shi*^{ts1}, was fitted well with three exponentials and had similar decay time constants (see legend to Figure 4B). The total number of quanta released when complete depletion was achieved in *shi*^{ts2} averaged 6.8 ± 0.3 × 10^4 (n = 5). Thus, although synaptic transmission in *shi*^{ts2} at 34°C is somewhat weaker than in *shi*^{ts1} at 32°C, the pattern of quantal content decline and transmission failure during prolonged tetanic stimulation were observed in common, indicating that these properties are specific to a mutation at the *shi* locus.

Effect of Stimulus Frequency on Quantal Content Decline Rates and on the Total Number of Quanta

The effect of stimulus frequency on the rates of quantal content decline, and on the total number of quanta released, was investigated in *shi*^{ts1} at the nonpermissive temperature. At the three frequencies studied (5, 10, and 20 Hz), the decline in quantal content during 4000 consecutive stimuli was well fitted with three exponentials (Figure 4A). Values obtained for slow (τ_1), intermediate (τ_2), and fast components (τ_3) of quantal content decline at 5, 10, and 20 Hz are shown in Figure 4B. As seen, slow (τ_1) and intermediate (τ_2) components were dependent on stimulus frequency.

At the nonpermissive temperature, the total number of quanta would not be expected to depend on the stimulus frequency. Complete exhaustion of synaptic transmission was achieved in the course of 4000 stimuli at 10 and 20 Hz (Figure 4A). The total number of quanta released at 20 Hz, obtained as described earlier for 10 Hz, averaged 8.5 ± 2.0 × 10^4 quanta (n = 5), which equals the total number of quanta obtained at 10 Hz (Figure 4C), indicating that, at the nonpermissive temperature, total quantal content does not depend on frequency of stimulation. At 5 Hz, synaptic depletion was not attained at the end of 4000 stimuli (Figure 4A). At this frequency the time constant of slow component was ~2,500 stimuli (Figure 4B). With this rate, only 80% of the slow component would be depleted after 4000 stimuli. At 32°C it was difficult to maintain cells under voltage control during the prolonged periods of time necessary to achieve depletion at 5 Hz (>20 min) and the total number of quanta could not be directly obtained at this frequency. After 4000 stimuli the number of quanta released at 5 Hz averaged 7.2 ± 0.6 × 10^4 quanta (n = 4). An estimate of vesicle content at 5 Hz can be obtained from these experimental data, assuming that 80% of depletion is achieved after 4000 stimuli and yields 9.0 ± 1.0 × 10^4 quanta (n = 5, blank column in Figure 4C).

Loading and Unloading of FM1-43 in RRP during Tetanic Stimulation at Nonpermissive Temperatures

In further work, we used the fluorescence imaging technique to investigate the rate of vesicle mobilization from RRP in *shi*^{ts1}. First, we confirmed with this technique the lack of endocytosis in *shi*^{ts1} and *shi*^{ts2} at nonpermissive temperatures (Figure 5A). Tetanic stimulation for 60 s at 10 Hz was used to load FM1-43 to the periphery of

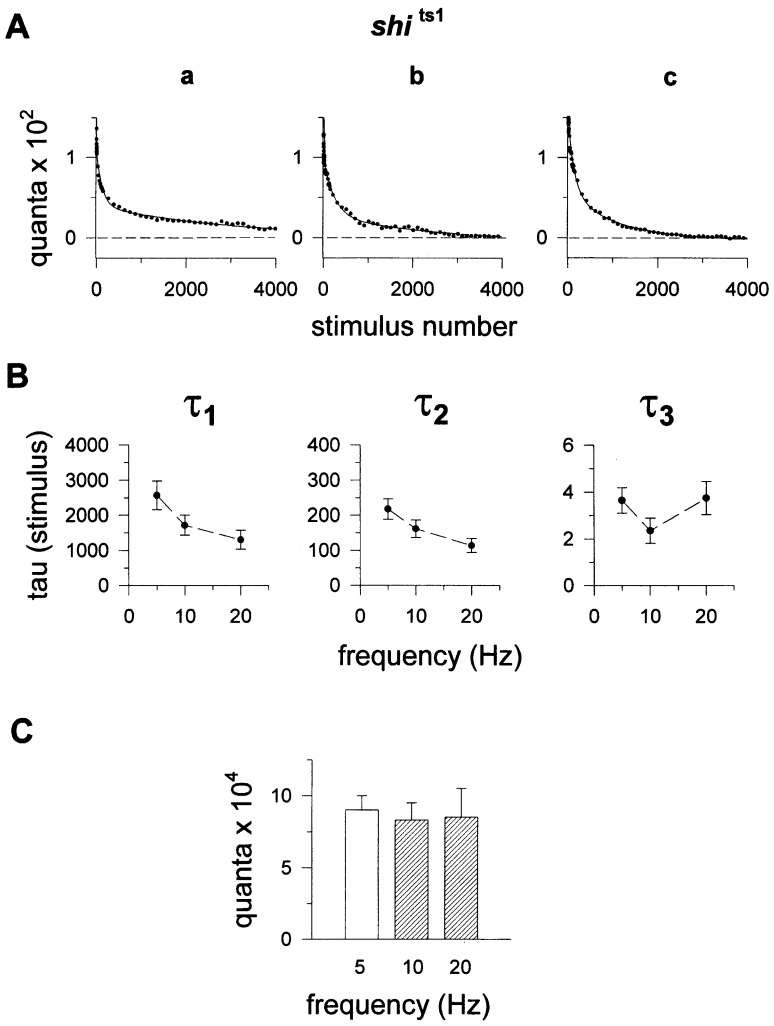

Figure 4. Analysis of Time Course of Decline in Quantal Content

(A) Time course of quantal content decline in *shi*^{ts1} at different stimulus frequencies. Representative examples of quantal content decay at 5 (Aa), 10 (Ab), and 20 Hz (Ac) stimulus frequency are depicted for initial 4000 stimuli. The continuous lines are the best fit of the following equation to the data:

$$Q_T = A_1 \exp(-T/\tau_1) + A_2 \exp(-T/\tau_2) + A_3 \exp(-T/\tau_3)$$

where Q_T is the quantal content at the T'th stimulus, T represents the stimulus number, the A's are constants in units of quanta, and τ's are time constants in the unit of stimulus. For clarity, one out of forty points were plotted.

(B) Graphs of slow (τ_1), intermediate (τ_2), and fast (τ_3) time constants of quantal content decline obtained in (A). Bars are SEM (5 Hz, n = 5; 10 and 20 Hz, n = 6). Similar fitting parameters were obtained in *shi*^{ts1} and *shi*^{ts2}. For example, at 10 Hz, *shi*^{ts1}: $\tau_1 = 1720 \pm 282$, $\tau_2 = 162 \pm 25$, $\tau_3 = 2.3 \pm 0.5$ (n = 6); *shi*^{ts2}: $\tau_1 = 2182 \pm 300$, $\tau_2 = 133 \pm 47$, $\tau_3 = 5.0 \pm 1.8$ (n = 3).

(C) Shaded columns are means of total number of quanta released at 10 and 20 Hz in *shi*^{ts1} at 32°C. Bar in each column is SEM (n = 6 for 10 and 20 Hz). Blank column represents the mean estimate of the total quanta at 5 Hz (n = 5).

synaptic boutons at room temperature (RRP, Figure 5Aa). Then, at nonpermissive temperatures (32°C for *shi*^{ts1}, 34°C for *shi*^{ts2}), partial unloading of the dye was induced by tetanic stimulation at 10 Hz for 30 s (Figure 5Ab). Following this maneuver, at nonpermissive temperatures, in the presence of FM1-43 in the external solution, the nerve was stimulated again at 10 Hz for 100 s. As shown in Figure 5Ac, FM1-43 was loaded in *CS*, but no dye loading was observed in *shi*^{ts1} or *shi*^{ts2}, showing that endocytosis was blocked at the nonpermissive temperatures in *shi*^{ts} mutants. Next, we examined backward mobilization of vesicles from RRP to RP. To this purpose, FM1-43 was first loaded in the periphery of synaptic boutons in *CS* and *shi*^{ts1} at 22°C (Figure 5Ba). The same preparations were then stimulated in standard external saline at 10 Hz for 100 s at 32°C. Finally, to observe fluorescence in the center, the dye in the periphery was unloaded by incubating the preparation for 5 min in high K^+ saline. As shown in Figure 5Bb, in *CS* fluorescence was observed in the center of boutons while no dye uptake at the center was detected in *shi*^{ts1}. This result documented that translocation of vesicles from RRP to RP is negligible in *shi*^{ts1} at the nonpermissive temperature.

The rate of forward mobilization of vesicles from RRP during tetanus was investigated in *shi*^{ts1} by measuring the decay of fluorescence intensity at the periphery of synaptic boutons. In these studies FM1-43 was loaded only to the periphery of boutons with tetanic stimulation for 60 s at room temperature (Figure 5Aa). After dye removal, temperature was raised to 32°C, nerves subjected to tetanic stimulation, and the loss of fluorescence was monitored. The time course of FM1-43 destaining at the periphery at different stimulus frequencies was well accounted for in terms of a single exponential component (Figure 5C). Time constants of FM1-43 destaining at the periphery of synaptic boutons derived from the slope of straight lines in Figure 5C (217 stimuli at 5 Hz; 196 stimuli at 10 Hz; 114 stimuli at 20 Hz) are similar to those of the second component of the time course of decline in quantal content during tetanus in *shi*^{ts1} at 32°C (τ_2 = 218 stimuli at 5 Hz; 162 stimuli at 10 Hz; 113 stimuli at 20 Hz; Figure 4B), indicating that it represents depletion of RRP. Since the time constants of optically determined destaining at the periphery of boutons and those of the second component in synaptic amplitude decline agree, no indication of "kiss and run" was detected in this experimental condition (Klingauf et al., 1998). The absence of a fast kinetic component (IRP) of FM1-43 destaining in the periphery of boutons, like

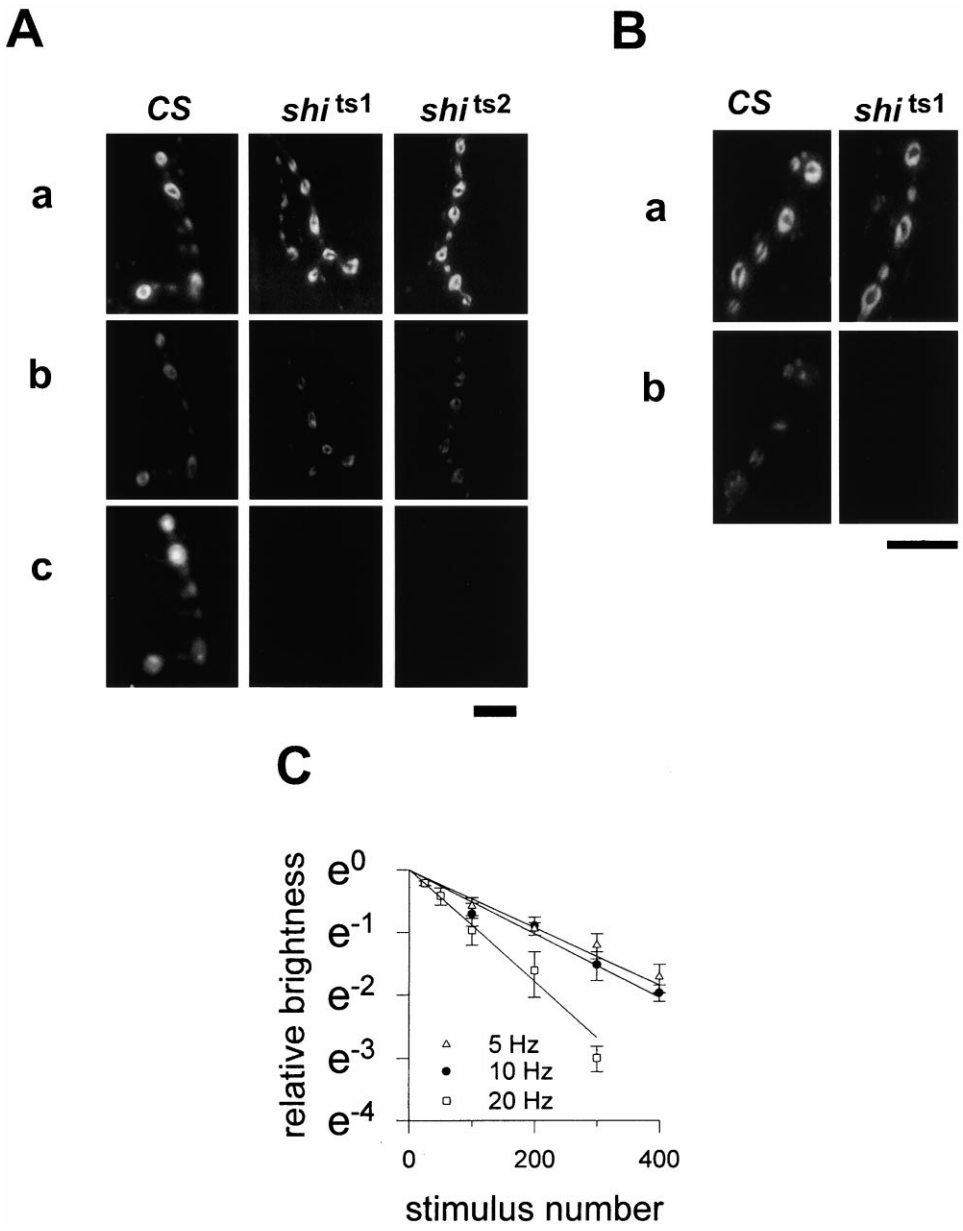

Figure 5. FM1-43 Staining and Destaining of Synaptic Boutons during Tetanic Stimulation

(A) Lack of endocytosis in *shi*^{ts} synaptic boutons at nonpermissive temperatures.

(Aa) Loading of FM1-43 to the periphery of synaptic boutons at room temperature was induced by tetanic stimulation at 10 Hz for 60 s in the presence of the dye.

(Ab) Partial unloading of FM1-43 from the periphery of synaptic boutons induced by tetanic stimulation at 10 Hz for 30 s at nonpermissive temperatures (32°C for *CS* and *shi*^{ts1}; 34°C for *shi*^{ts2}) in the absence of dye in the external solution.

(Ac) Images of synaptic boutons obtained after tetanic stimulation at 10 Hz for 100 s at nonpermissive temperatures in the presence of FM1-43. Note that synaptic boutons in *CS* exhibit FM1-43 staining, but no staining is seen in *shi*^{ts1} and *shi*^{ts2}. The scale bar is 10 μm.

(B) Lack of vesicle translocation from RRP to RP in *shi*^{ts1} at 32°C.

(Ba) FM1-43 staining into the periphery of synaptic boutons was induced as in (Aa).

(Bb) After dye removal from the external solution, temperature was raised to 32°C and preparations stimulated at 10 Hz for 100 s. Finally, preparations were incubated in high K^+ solution for 5 min at 32°C to unload dye from the periphery of boutons. In *CS* (lower left photograph), FM1-43 fluorescence is observed in the center of boutons. In *shi*^{ts1} (lower right photograph), no fluorescence was detected in the center. The scale bar is 10 μm.

(C) Time course of FM1-43 destaining at the periphery of synaptic boutons during tetanic stimulation. Loading of the periphery of synaptic boutons with FM1-43 was achieved as in (Aa). Following loading, dye was washed out from the external solution, temperature elevated to 32°C, and fluorescence intensity measured at $t = 0$. Tetanic stimulation at 5, 10, or 20 Hz was then initiated. Fluorescence remaining at the periphery of same boutons at a given time interval was measured. In the graph, fluorescence intensity at each time interval relative to intensity at $t = 0$ (in the natural logarithmic scale) is plotted against stimulus number at different stimulus frequencies. Bar attached to each symbol is SEM. Each experimental point at each frequency in the graph was derived from 4–6 different larvae, and at least 10 boutons were measured

that recorded electrophysiologically (see for example Figure 4B), indicates that vesicles in IRP are few and that depletion of IRP is not resolved in our imaging studies.

Cytochalasin-D Inhibited Mobilization of Vesicles from RP during Tetanic Stimulation

To estimate the size of RRP, we needed to block recruitment of vesicles from RP. To this end, we examined in *shi*^{ts1} the effects of cyt-D treatment on the unloading process of FM1-43 from the central region during tetanic stimulation at 32°C. As shown in Figures 6A1–6D1, high K^+ depolarization for 5 min at room temperature, in the presence of FM1-43, loaded the dye predominantly in the periphery of boutons. When such maneuver was followed by tetanic stimulation at 10 Hz for 5 min in the presence of FM1-43 at room temperature, loading of the dye to the central region of boutons was observed (Figures 6A2–6D2). After the dye was washed out, a second K^+ depolarization unloaded the dye at the periphery (RRP) but left a substantial amount of staining at the center (RP, Figures 6A3–6D3). Further tetanic stimulation at nonpermissive temperature for 5 min at 10 Hz unloaded most of FM1-43 from the center in the controls (Figures 6A4 and 6B4) but left large fraction of staining in boutons treated with cyt-D (Figures 6C4 and 6D4), suggesting that cyt-D treatment inhibited translocation of vesicles from RP.

The time course of FM1-43 unloading from the center of synaptic boutons in cyt-D-treated preparations and in the controls was investigated (Figure 6E). In the controls, decay time constants for FM1-43 destaining at the center of synaptic boutons were 1400 ± 90 stimuli (n = 3) and 1110 ± 160 stimuli (n = 6) at 10 and 20 Hz, respectively (Figure 6E). These rates agree well with the decay time constants of the slow component of quantal content decline in Figure 4 (τ_1 = 1720 stimuli at 10 Hz, 1308 stimuli at 20 Hz), indicating that, at 32°C, availability of vesicles for release in the late phase of tetanic stimulation is limited by the rate of vesicle mobilization from RP. Since at 32°C backward mobilization of vesicles is undetectable (Figure 5B), these rates represent forward translocation rates from RP to RRP. In cyt-D-treated boutons, rates of FM1-43 destaining at the center (8700 ± 1400 stimuli, n = 5 at 10 Hz and 5140 ± 690 stimuli, n = 5, at 20 Hz; Figure 6E) were significantly slower relative to the controls (Figure 6E), showing that cyt-D treatment inhibited vesicle translocation from RP.

The slow rates of vesicle translocation from RP to RRP in cyt-D-treated preparations (1/8700 per stimulus at 10 Hz, 1/5140 per stimulus at 20 Hz; Figure 6E) relative to the much faster rates of mobilization of RRP (1/196 per stimulus at 10 Hz; 1/114 per stimulus at 20 Hz; Figure 5C) predict that, at these frequencies, 600–800 stimuli would suffice to deplete RRP, while during this period the number of vesicles translocated from RP per stimulus would remain nearly constant. F(T), the rate of vesicle fusion per stimulus as a function of stimulus number at 10 Hz, was simulated for cyt-D-treated boutons under three conditions (Figure 6F). The filled circles describe the time course of vesicle fusion when RP is empty ($[RP]_0 = 0$). The open circles represent the case when RRP is empty ($[RRP]_0 = 0$) and depicts the contribution of RP to vesicle release in cyt-D-treated synaptic boutons. For comparison, the contribution of RP to quantal release when RRP is empty for boutons not treated with cyt-D is depicted also (open triangles). Finally, the time course of quantal release in boutons treated with cyt-D when both RP and RRP are present is described by the continuous line in Figure 6F. In this case, after a fast decline phase, due to IRP plus RRP depletion, the rate of vesicle release reaches a quasi steady state at which quanta are released at a low rate. Thus, in cyt-D-treated neuromuscular junctions in *shi*^{ts1} at 32°C, quantal content of IRP plus RRP can be estimated from experimental records by subtracting the nearly constant contribution leaking out of RP.

Estimation of Pool Sizes

The time course of synaptic current amplitude decline during 10 Hz tetanic stimulation in *CS* at 32°C following cyt-D treatment (Figure 7A, right panel) was similar to that of the control (Figure 7A, left panel). At the steady state, cyt-D-treated neuromuscular junctions released transmitter at a rate of 54 ± 13 quanta/stimulus (n = 8) compared to 66 ± 12 quanta/stimulus in the control. Thus, when vesicles are recycling, RP contributes only modestly to transmitter release.

On the other hand, as predicted in Figure 6F, in *shi*^{ts1} motor endplates treated with cyt-D at 32°C, transmitter release decayed rapidly, within 600 stimuli, to a low, nearly constant rate of 7.6 ± 2.0 (n = 5) quanta per stimulus at 10 Hz and 17.0 ± 3.0 quanta per stimulus (n = 5) at 20 Hz (Figure 7C). Quanta released during this period averaged 1.5 ± 0.3 × 10^4 (n = 5), at 10 Hz and 2.6 ± 0.6 × 10^4 at 20 Hz (n = 5). Subtracting the steady-state leak from the total number of quanta released, $[RRP]_0 + [IRP]_0$ = 1.1 ± 0.2 × 10^4 quanta (n = 5) at 10 Hz and 1.6 ± 0.4 × 10^4 quanta (n = 5) at 20 Hz. Since the total number of quanta at 10 Hz was estimated earlier at 8.3 × 10^4 quanta at 10 Hz and 8.5 × 10^4 quanta at 20 Hz, the total number of quanta in RRP and IRP amounts to 14%–20% of all quanta.

At 10 Hz, the time course of decline of quantal content in cyt-D-treated preparations was fitted well with two exponentials and a steady-state component, with decay constants of 2.4 ± 0.2 stimuli and 220 ± 14 stimuli (n = 5). At 20 Hz, decay times were 4.9 ± 1.8 stimuli and 141 ± 13 stimuli (n = 5). At both frequencies, the time constant of the second component is close to that of FM1-43 destaining rates from the periphery of boutons described in an earlier section (196 stimuli at 10 Hz; 114 stimuli at 20 Hz).

Analysis of the Time Course of Quantal Content Decline at 32°C in *shi*^{ts1} Treated with cyt-D

To obtain estimates of pool sizes using an independent approach, the time course of quantal content decline

in each larvae. Background fluorescence, defined as that residual fluorescence remaining after 5 min in the high K^+ solution, was subtracted from each measured fluorescence intensity. Straight lines are best fits with slopes of 217 stimuli for 5 Hz (r^2 = 0.99, regression coefficient); 196 stimuli for 10 Hz (r^2 = 0.99); and 114 stimuli at 20 Hz (r^2 = 0.99).

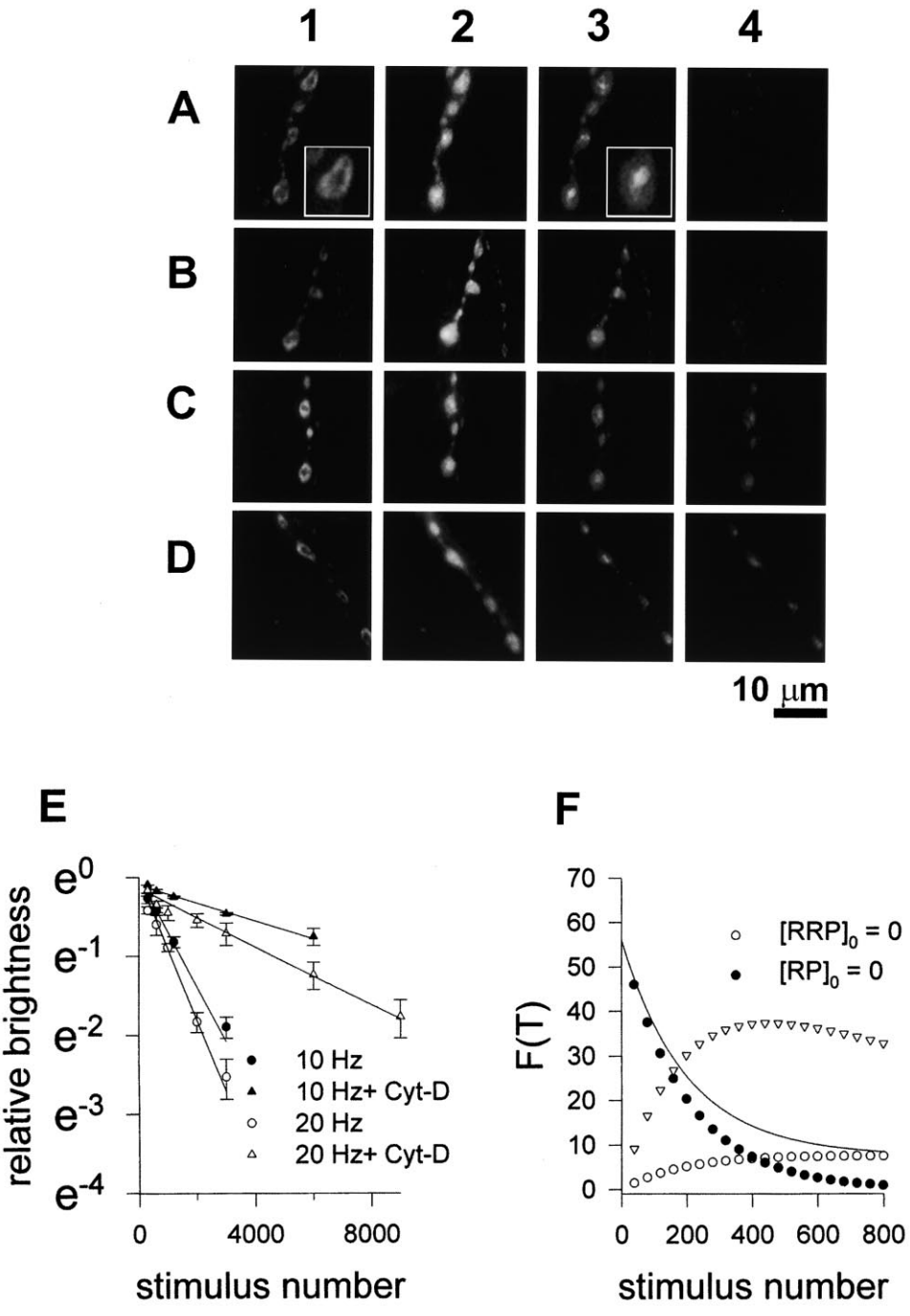

Figure 6. Effect of Cyt-D Treatment on the Time Course of FM1-43 Destaining at the Center of Synaptic Boutons in *shi*^{ts1}

Images 1–4 are from the same set of synaptic boutons.

(A and B) Controls. (1) Staining pattern of synaptic boutons following high K^+ treatment in the presence of FM1-43 in the external solution at room temperature. The inset presents an enlarged image of a synaptic bouton to further document that high K^+ treatment loads FM1-43 to the periphery (RRP). (2) Following high K^+ treatment, the sample was washed extensively with standard solution and subjected to tetanic stimulation for 5 min at 10 Hz in the presence of FM1-43. Then, the sample was washed extensively with FM1-43-free standard saline prior to image acquisition. (3) High K^+ treatment for 5 min in FM1-43-free solution unloaded the dye from the periphery of boutons (RRP) but left a substantial amount of fluorescence at the center region of boutons (RP). For clarity, the inset shows an enlarged image of a synaptic bouton obtained under these experimental conditions. (4) Temperature was raised to 32°C and preparations subjected to tetanic stimulation at 10 Hz for 5 min, causing the loss of FM1-43 staining at the center of boutons.

(C and D) Same series of experiments as (A and B) following cyt-D treatment between (3) and (4). In cyt-D-treated boutons, a sizeable amount of fluorescence remained at the center of synaptic boutons after tetanic stimulation at 10 Hz for 5 min.

(E) Relative brightness at the center of synaptic boutons (in the natural logarithmic scale) is plotted against stimulus number for controls and for cyt-D-treated preparations. To build the graph, images of same boutons were captured at $t = 0$ and at different times during tetanic stimulation. Fluorescence intensity was then measured off line from same area at the center of each synaptic bouton. Each point in the graph

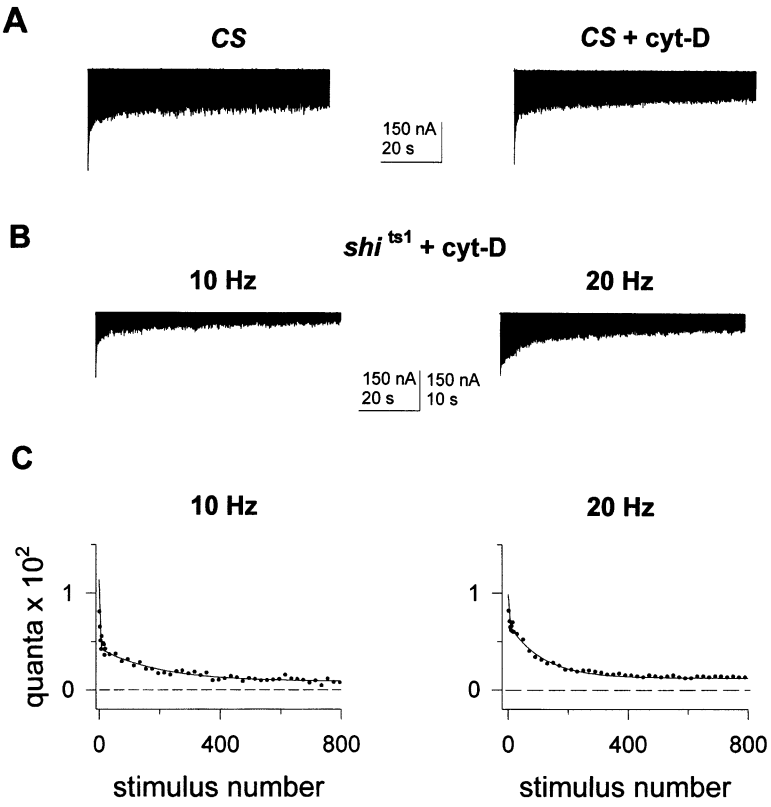

Figure 7. Analysis of Decline of Synaptic Current Amplitudes during Tetanus at 32°C after Cyt-D Treatment

(A) Representative examples of evoked synaptic currents in response to stimulation at 10 Hz in *CS* without treatment with cyt-D (left panel) and *CS* after cyt-D treatment (right panel).

(B) Records of evoked currents in cyt-D-treated *shi*^{ts1} neuromuscular junctions at 32°C at 10 and 20 Hz.

(C) Quantal content of evoked currents in (B) versus stimulus number. For clarity only one out of 10 points was plotted; the solid line is the best fit of Equation 3 to data. For the experiment at 10 Hz shown in (B), quantal content of first evoked current ($[IRP]_0 \times k_3$) was 125 quanta. At steady state, the rate of quantal release ($[RP]_0 \times k_1$) was 7 quanta per stimulus. Parameters for the best fit at 10 Hz were as follows: $k_3 = 0.34$ stimuli^{-1}, $[IRP]_0 = 370$ quanta, $[RRP]_0 = 1.0 \times 10^4$ quanta, $[RP]_0 = 6.1 \times 10^4$ quanta. In the experiment at 20 Hz shown in (B), 100 quanta were released at the first stimulus; the steady-state release rate was 12 quanta/stimulus, and the parameters for the best fit were as follows: $k_3 = 0.7$ stimuli^{-1}, $[IRP]_0 = 143$ quanta, $[RRP]_0 = 8.0 \times 10^3$ quanta, and $[RP]_0 = 6.4 \times 10^4$ quanta.

during tetanic stimulation in cyt-D-treated preparations at 32°C was analyzed. To this purpose, vesicle depletion at *shi*^{ts1} neuromuscular junctions treated with cyt-D was represented with the following scheme:

$$RP \xrightarrow{k_1} RRP \xrightarrow{k_2} IRP \xrightarrow{k_3} F, \quad (1)$$

where k's represent forward rate constants and F fusion events. k_1 and k_2, the forward rate constants for RP and RRP were derived from optical measurements (Figures 5 and 6) and used in the analysis to reduce the number of free parameters. Backward mobilization of vesicles from RRP to RP was not considered in Scheme 1 based on results shown in Figure 5B. In addition, backward mobilization of vesicles from IRP to RRP was ignored in the scheme considering that in this situation boutons are being rapidly depleted of vesicles and forward movement of vesicles is predominant.

In Scheme 1, the quantal content per stimulus is given by the number of vesicles in IRP at the T'th stimulus ([IRP](T)) multiplied by k_3. Scheme 1 leads to the following expressions:

$$d[RP](T)/dT = -[RP](T) \times k_1$$
$$d[RRP](T)/dT = [RP](T) \times k_1 - [RRP](T) \times k_2$$
$$d[IRP](T)/dT = [RRP](T) \times k_2 - [IRP](T) \times k_3$$

We are interested in representing quantal content decline during 600 stimuli, which is small compared with the decay time constants of RP depletion (8700 stimuli at 10 Hz and 5140 stimuli at 20 Hz stimulation). Thus, we can safely assume that the rate of translocation from RP is constant and given by RP $\times$ k_1 (Figure 6F). With

was built by averaging the relative fluorescence intensity of many boutons from at least three different preparations at the T'th stimulus. Lines joining experimental points are best fit of straight line to data points.

(F) Simulation of quantal release during tetanic stimulation in the cyt-D-treated preparation at nonpermissive temperature. Since movement of vesicles from RRP to RP is absent in cyt-D-treated neuromuscular junctions, synaptic vesicle depletion is represented in the following scheme:

$$RP \xrightarrow{k_1} RRP \xrightarrow{k_2} F,$$

where k_1 and k_2 are rate constants obtained, in Figure 5, 1/196 stimuli^{-1} at 10 Hz for k_2 and, in Figure 6, 1/8700 stimuli^{-1} at 10 Hz for k_1. For simplicity, IRP is omitted in the scheme. F denotes fusion events. Solving for [RRP](T), the number of vesicles in RRP at T'th stimulus, will be:

$$[RRP]_T = [RRP]_0 \exp(-k_2 T) + \left\{k_1[RP]_0 / (k_2 - k_1)\right\}\{\exp(-k_1 T) - \exp(-k_2 T)\}$$

where $[RRP]_0$ and $[RP]_0$ are the size of RRP and RP at T = 0 and T is stimulus number. In the simulation, we used values obtained in depletion experiments described previously at 10 Hz stimulus frequency ($[RP]_0 = 7.2 \times 10^4$; $[RRP]_0 = 1.1 \times 10^4$).

this consideration, solving for [IRP](T), we obtained the following expression;

$$[IRP](T) = A_0\left[\left(k_1 / k_3\right)\{1 - \exp(-k_3T)\} + \left\{k_1 / (k_3 - k_2)\right\}\{\exp(-k_3T) - \exp(-k_2T)\}\right] + B_0\left\{k_2 / (k_3 - k_2)\right\}\{\exp(-k_2T) - \exp(-k_3T)\} + C_0 \exp(-k_3T), \quad (2)$$

where A_0, B_0, and C_0 are constants. Since the rate of release from IRP is much faster than the rate of mobilization of RRP, $k_3 >> k_2$, and $k_3 - k_2 \approx k_3$. With this consideration, the following expression will account for (Q_T), the quantal content at the T'th stimulus:

$$Q_T = \{[IRP]_0 k_3 \exp(-k_3T)\} + [RRP]_0 k_2 \{\exp(-k_2T) - \exp(-k_3T)\} - [RP]_0 k_1 \exp(-k_2T) + [RP]_0 k_1, \quad (3)$$

where $[IRP]_0$, $[RRP]_0$, and $[RP]_0$ are the sizes of IRP, RRP, and RP at $t = 0$. $[IRP]_0 \times k_3$ is the quantal content of the first evoked synaptic current. The product $[RP]_0 \times k_1$ represents the quasi steady-state rate of quantal release. Using k_1 obtained from imaging studies, $[RP]_0$, the number of vesicles in RP at $t = 0$, can be estimated directly from the values for the steady state quantal content in *shi*^{ts1} cyt-D-treated preparations, yielding $6.5 \pm 1.3 \times 10^4$ quanta at 10 Hz ($n = 5$) and $7.3 \pm 0.7 \times 10^4$ at 20 Hz ($n = 5$). Estimates for k_3 and $[RRP]_0$ are obtained by adjusting Equation 3 to fit the data shown in Figure 7C, with k_1, k_2, $[RP]_0$, and $[IRP]_0 \times k_3$ fixed. The analysis of data at 10 Hz yielded the following: $k_3 = 0.5 \pm 0.02$ stimuli^{-1}, $[IRP]_0 = 230 \pm 25$ quanta, and $[RRP]_0 = 1.1 \pm 0.1 \times 10^4$ quanta ($n = 5$); at 20 Hz: $k_3 = 0.6 \pm 0.2$, $[IRP]_0 = 297 \pm 107$, $[RRP]_0 = 1.2 \pm 0.2 \times 10^4$ ($n = 5$). The total number of quanta derived from the analysis amounted to $8.0 \pm 1.4 \times 10^4$ ($n = 5$) and $8.5 \pm 1.0 \times 10^4$ ($n = 5$) quanta at 10 and 20 Hz, respectively. Within experimental error, $[RRP]_0$, $[RP]_0$, and the total number of quanta obtained from this analysis agree well with those derived directly from depletion experiments. Moreover, the analysis indicates that the quantal content of $[IRP]_0$ is small compared to $[RRP]_0$ and $[RP]_0$.

Discussion

Vesicle Pools

Birks and MacIntosh (1961) first suggested that releasable acetylcholine in the cat cervical ganglion is compartmentalized into two pools, a small readily releasable pool (RRP) and a larger less-releasable one. Since then, two pools of synaptic vesicles have been documented in various preparations (Zimmermann and Whittaker, 1977; Pieribone et al., 1995). In hippocampal neurons, Rosenmund and Stevens (1996) defined the RRP as a set of vesicles released by hypertonic solutions and presented evidence that during evoked synaptic currents vesicles are drawn from this pool.

In bovine adrenal chromaffin cells, Neher and Zucker (1993) proposed a model for vesicle secretion with three pools, namely, depot pool, nearly releasable pool, and immediately releasable pool. Following Neher and Zucker (1993), we termed the fast component in quantal decline observed at all stimulus frequencies in electrophysiological studies the "immediately releasable pool" (IRP). Under the experimental conditions used here (2 mM external Ca^{2+}), half of IRP is depleted rapidly within a few stimuli. It might represent vesicles docked and primed at release sites.

In *Drosophila* terminals, Koenig and Ikeda (1996) suggested the presence of two pools of synaptic vesicles, with different characteristics and functions. At larval *Drosophila* neuromuscular junctions, Kuromi and Kidokoro (1998) identified two vesicle pools and called them "exo/endo cycling and reserve pools." The RP in the present work corresponds to their "reserve pool," while their "exo/endo cycling pool" includes both IRP and RRP. Here, RRP and RP are basically defined by properties revealed in FM1-43 staining experiments. IRP was defined electrophysiologically and associates with the initial fast component in quantal content decline. Thus, our results are consistent with three pools of synaptic vesicles at *Drosophila* larvae motor endplates, namely IRP, RRP, and RP.

Recycling Rates of Synaptic Vesicles during Tetanic Stimulation

At room temperature, after ~100 s of tetanic nerve stimulation at 10 Hz, synaptic current amplitude attained a steady level both in *CS* and *shi*^{ts1} (Figure 1A). The recycling rate can be estimated from this steady-state level. Recycling increased with frequency, reaching a maximum rate of 1000 quanta/s (Figure 2C), which was similar at 32°C. Taking the total number of release sites on muscle #6 or #7 as ~550 (Atwood et al., 1993), less than two vesicles would be recycled per s at each release site.

Effects of Cyt-D on Vesicle Mobilization

Cyt-D prevents actin polymerization (Cooper, 1987). In *shi*^{ts1}, Kuromi and Kidokoro (1998) showed that cyt-D blocks the formation of RP at room temperature after depletion of vesicles at 32°C. In the present study, inhibition of FM1-43 destaining at the center of boutons in *shi*^{ts1} at nonpermissive temperature after pretreatment with cyt-D was demonstrated (Figures 6C and 6D), revealing that actin polymerization plays a role in the translocation of vesicles from RP. This action of cyt-D provided us a useful tool to estimate the size of RRP.

Estimation of Vesicle Pool Sizes by Depletion Experiments

At nonpermissive temperatures, all synaptic vesicles can be depleted in *shi* (Koenig and Ikeda, 1989, 1996; Koenig et al., 1989; Estes et al., 1996), and consequently the total quantal content can be directly quantified in electrophysiological studies. Here, we documented vesicle depletion in two *shi* alleles (*shi*^{ts1} and *shi*^{ts2}) and showed that, in the absence of recycling, the total number of quanta (8.4×10^4) does not depend on stimulus frequency.

When endocytosis is blocked and translocation of vesicles from RP is inhibited by cyt-D, RRP should be the main source of vesicles for synaptic transmission. The number of quanta released at 32°C, after cyt-D treat-

ment, decayed to a low steady state at which neurotransmitter continued to be released at a low rate, due to slow translocation of vesicles from RP. Subtraction of the residual release allowed us to estimate of the size of RRP at 1.1–1.6 $\times$ 10^4 quanta (ignoring small IRP), which would comprised 14%–19% of all quanta available. The 1:5–1:7 RPP/RP ratio obtained in this work agreed well with the 1:6 ratio reported by Kuromi and Kidokoro (1998) using a different approach.

Estimation of Vesicle Pool Sizes from Kinetics of Decline in Quantal Content during Tetanic Stimulation

The time course of quantal content decay during tetanic stimulation in *shi*^{ts1} at 32°C after cyt-D treatment was analyzed with Scheme 1. Using estimates for forward mobilization rates for RP and RRP pools obtained in imaging experiments, Equation 3 was fitted to experimental data with only two free parameters, $[RRP]_0$ and k_3. Estimates for RRP and RP agreed well with those derived from the depletion experiments described above. The analysis corroborated that IRP is small and fits with the idea that this pool represents docked and primed vesicles at release sites. Assuming that there are 550 release sites at the larval neuromuscular junction (Atwood et al., 1993), less than half of release sites have one docked and primed vesicle.

Two Types of Terminals on Muscles #6 and #7

It is known that abdominal muscles #6 and #7 are innervated by two types of axon, type Ib with large varicosities and Is with smaller ones. Each varicosity has multiple synapses (41 for Ib and 7 for Is) and each synapse has on average one presynaptic release site. The total number of synapses has been estimated to be 350–450 for Ib and 100–200 for Is (Atwood et al., 1993). In HL-3 medium (Stewart et al., 1994), type Is boutons produced larger synaptic potentials, and extracellularly recorded currents from type Is boutons had faster decay times (Kurdyak et al., 1994). The probabilities of vesicle release from these two types of boutons were also different in HL3 medium (Atwood et al., 1997).

Since these two types of nerve could not be separated by stimulus intensity (Kurdyak et al., 1994), we used stimulus intensities strong enough to obtain maximum synaptic currents. Thus, in our experiments, both types of nerve must have been activated. Furthermore, under the experimental conditions used (2 mM Ca^{2+} in the external solution), the quantal content of synaptic currents was saturated since it did not increase further by raising external Ca^{2+} above 2 mM. Under this condition, both types of terminal must behave similarly during depletion induced by tetanic nerve stimulation.

Adult *shibire* Flies Are More Susceptible to High Temperatures Than Larvae

In this study, we have used the larval neuromuscular junction as a model of synapses and estimated the size of vesicle pools and the recycling rate. However, it should be noted that the size of vesicle pools and recycling rate could be substantially different among synapses. It is known that *shibire* flies paralyze more quickly at nonpermissive temperatures than larvae and recover from paralysis within a few minutes at room temperature. Koenig and Ikeda (1996) have reported in *shi*^{ts1} that in the synapse between photoreceptor cells and interneurons in the optic ganglion, vesicle depletion occurs within 30 s upon light stimulation at 29°C. At the neuromuscular junction of adult *shi*^{ts1} flies, the same investigators have shown that it takes more than 480 s at 0.5 Hz nerve stimulation for depletion (240 stimuli; Koenig and Ikeda, 1989). In contrast, at larval neuromuscular junctions, it has been demonstrated in EM that vesicle depletion occurs within 5 min in high K^+ saline at 34°C in *shi*^{ts1} (Estes et al., 1996). In this study, we have also observed that it takes more than 150 s at 20 Hz (3000 stimuli) to exhaust synaptic transmission at 32°C. It is possible that the vesicle pools in synapses in the central nervous system or in some neuromuscular junctions of adult flies are smaller than those at the larval neuromuscular junctions. Also, it appears that higher temperatures are required to stop recycling at larval neuromuscular junctions than at synapses in adult flies.

Experimental Procedures

Fly Stocks

A temperature-sensitive paralytic mutant, *shibire*, *shi*^{ts1}, and *shi*^{ts2}, and wild-type *Canton S* (*CS*) were used in this study. The stock flies were bred either at 18.5°C (*shi*^{ts1} and *shi*^{ts2}) or at 22°C (*CS*) on the standard cornmeal medium supplemented with yeast.

Electrophysiology

Evoked postsynaptic currents were recorded from ventral longitudinal muscle #6 or #7 at abdominal segment A2 or A3 (Campos-Ortega and Hartenstein, 1985) using a two-microelectrode voltage-clamp (OC-725, Warmer Instruments, Hamden, CT) at −80 mV holding potential (Acharya et al., 1998). Except when indicated, all experiments were performed in a standard solution made of (in mM): 128 NaCl; 2 KCl; 4 $MgCl_2$; 2 $CaCl_2$; 5 HEPES; 36 sucrose; pH 7.3. For stimulation, nerves were cut close to the ventral ganglion and sucked into a pipette filled with standard solution. The nerve was stimulated at frequencies indicated in each experiment using a programmable stimulator (Master-8, A. M. P. I., Jerusalem, Israel). Data acquisition and analysis were performed using pClamp software (Axon Instruments, Foster City). To measure the amount of charge transfer during synaptic transmission, semiautomatic integration of individual evoked currents was done with software written by Dr. J. C. Letelier. Fittings were performed using Nfit software (University of Texas, Galveston, TX).

Loading and Unloading of FM1-43

Loading of synaptic boutons with FM1-43 was achieved by treatment with the high K^+ solution (90 mM KCl) or by tetanic stimulation in the presence of the dye in the standard solution. Loading was carried out for periods indicated in the respective figure legend. In all cases, [FM1-43] in the external solution was 5 μM. Dye removal was performed by vigorous rinsing with dye-free standard solution. Unloading of FM1-43 from synaptic boutons was achieved by treatment with the high K^+ solution or by tetanic stimulation as indicated in the respective figure legend.

Fluorescence Imaging

Synaptic boutons were visualized using a 60$\times$ objective on an Olympus microscope (BX50WI) equipped with epifluorescence. Images of boutons were captured by a Cohu video camera (Cohu, San Diego, CA) at a rate of 0.03 s/frame, in an "on-chip" integration mode, commanded and digitized by a Scion frame grabber card, and analyzed using Scion software (Scion, MA). In all cases, the integral of 15 frames was analyzed. Prior to image acquisition, synaptic boutons in chosen muscle segments were located promptly using Hoffman Optics with low illumination intensity. Next, samples were excited and images of boutons captured under the condition

in which boutons were exposed to excitation light, at most 10 s in each sampling period. For convenience, all measurements reported here were done in larger boutons (2–3 μm in diameter) and the fluorescence intensity of at least 10 boutons were measured in each preparation. Controls showed that bleaching between two successive samplings amounted 1.3% ± 0.3%. Quantitative analysis of brightness was made after correcting for bleaching and background.

Cytochalasin-D Treatment of Synaptic Boutons

For imaging studies, the center of synaptic boutons was loaded first at room temperature with FM1-43 as explained in the corresponding figure legend. Then, preparations were exposed to high K^+ solution for 5 min to destain FM1-43 from RRP. Following this procedure, most of FM1-43 staining was confined to the center of boutons (RP) (Figures 6A3–D3). After dye removal, the external medium was replaced by the standard solution containing 10 μM cyt-D. The preparation was kept in this solution for 10 min and then washed extensively with cyt-D-free standard solution. Fluorescence intensity from the central region of boutons, corrected for background and bleaching, was defined as the intensity at $t = 0$. Nerves were stimulated at the indicated frequencies, and the fluorescence intensity at the center region of boutons was measured at different times during tetanic stimulation. The intensity of fluorescence, corrected for background and bleaching, was expressed as the fraction of the fluorescence intensity remaining at the i^{th} stimulating episode relative to that measured at $t = 0$. Controls were subjected to same treatment, except that the incubation in cyt-D was replaced by 10 min incubation in standard solution.

For electrophysiological studies, preparations were incubated for 10 min in 10 μM cyt-D. After extensive rinsing with cyt-D-free solution, temperature was elevated to 32°C and nerves subjected to tetanic stimulation for periods specified in the corresponding figure legend. Controls were subjected to the identical treatment, except that incubation in cyt-D was replaced by 10 min incubation in standard solution.

Chemicals

FM1-43 was obtained from Molecular Probes (Eugene, OR). FM1-43 was dissolved in 100% ethanol at the concentration of 10 mM as a stock solution. Cytochalasin-D was purchased from Sigma (St Louis, MO).

Acknowledgments

Supported by FONDECYT, HHMI, and a Catedra Presidencial en Ciencias (to P. L.) and by a grant-in-aid from the Ministry of Education, Science, Sports, and Culture of Japan (to Y. K.). Institutional support from Fuerza Area de Chile and a group of Chilean Companies (AFP Provida, CGE, CODELCO, Empresas CMPC, Gener S. A., Minera Collahuasi, Minera Escondida, Novagas, Business Design Associates, and Xerox Chile) is recognized. C. E. C. S. is a Millenium Science Institute. P. L. is an International Scholar of the HHMI.

Received March 20, 2000; revised September 5, 2000.

References

Acharya, J.K., Labarca, P., Delgado, R., Jalink, K., and Zuker, C.S. (1998). Synaptic defects and compensatory regulation of inositol metabolism in inositol polyphosphate 1-phosphatase mutants. Neuron *20*, 1219–1229.

Atwood, H.L., Govind, C.K., and Wu, C.-F. (1993). Differential ultrastructure of synaptic terminals of ventral longitudinal abdominal muscles in *Drosophila* larvae. J. Neurobiol. *24*, 1008–1024.

Atwood, H.L., Karunanithi, S., Georgiou, J., and Charlton, M.P. (1997). Strength of synaptic transmission at neuromuscular junctions of crustaceans and insects in relation to calcium entry. Invert. Neurosci. *3*, 81–87.

Betz, W.J., and Bewick, G.S. (1992). Optical analysis of synaptic vesicle recycling at the frog neuromuscular junction. Science *255*, 200–203.

Birks, R., and MacIntosh, R.C. (1961). Acetylcholine metabolism of a sympathetic ganglion. Can. J. Biochem. Physiol. *39*, 787–827.

Campos-Ortega, J.A., and Hartenstein, V. (1985). The Embryonic Development of *Drosophila melanogaster* (New York: Springer).

Cooper, J.A. (1987). Effects of cytochalasin and phalloidin on actin. J. Cell Biol. *105*, 1473–1478.

De Camilli, P., and Takei, K. (1996). Molecular mechanisms in synaptic vesicle endocytosis and recycling. Neuron *16*, 481–486.

Estes, P.S., Roos, J., van der Bliek, A., Kelly, R.B., Krishnan, K.S., and Ramaswami, M. (1996). Traffic of dynamin within individual *Drosophila* synaptic boutons relative to compartment-specific markers. J. Neurosci. *16*, 5443–5456.

Heuser, J.E., and Reese, T.S. (1973). Evidence for recycling of synaptic vesicle membrane during synaptic transmission at the frog neuromuscular junction. J. Cell Biol. *57*, 315–344.

Jan, L.Y., and Jan, Y.N. (1976). Properties of the larval neuromuscular junction in *Drosophila melanogaster*. J. Physiol. Lond. *262*, 189–214.

Klingauf, J., Kavalali, E.T., and Tsien, R.W. (1998). Kinetics and regulation of fast endocytosis at hippocampal neurons. Nature *394*, 581–585.

Koenig, J.H., and Ikeda, K. (1989). Disappearance and reformation of synaptic vesicle membrane upon transmitter release observed under reversible blockage of membrane retrieval. J. Neurosci. *9*, 3844–3860.

Koenig, J.H., and Ikeda, K. (1996). Synaptic vesicles have two distinct recycling pathways. J. Cell Biol. *135*, 797–808.

Koenig, J.H., Kosaka, T., and Ikeda, K. (1989). The relationship between the number of synaptic vesicles and the amount of transmitter released. J. Neurosci. *9*, 1937–1942.

Kurdyak, P., Atwood, H.L., Stewart, B.A., and Wu, C.F. (1994). Differential physiology and morphology of motor axons to ventral longitudinal muscles in larval *Drosophila*. J. Comp. Neurol. *350*, 463–472.

Kuromi, H., and Kidokoro, Y. (1998). Two distinct pools of synaptic vesicles in single presynaptic boutons in a temperature-sensitive *Drosophila* mutant, *shibire*. Neuron *20*, 917–925.

Kuromi, H., and Kidokoro, Y. (1999). The optically determined size of exo/endo cycling vesicle pool correlates with the quantal content at the neuromuscular junction of *Drosophila* larvae. J. Neurosci. *19*, 1557–1565.

Kuromi, H., and Kidokoro, Y. (2000). Tetanic stimulation recruits vesicles from reserve pool via a cAMP-mediated process in *Drosophila* synapses. Neuron *27*, 133–143.

Neher, E., and Zucker, R.S. (1993). Multiple calcium-dependent processes related to secretion in bovine chromaffin cells. Neuron *10*, 21–30.

Pieribone, V.A., Shupliakov, O., Brodin, L., Hilfiker-Rothenfluh, S., Czernik, A.J., and Greengard, P. (1995). Distinct pools of synaptic vesicles in neurotransmitter release. Nature *375*, 493–497.

Rosenmund, C., and Stevens, C.F. (1996). Definition of the readily releasable pool of vesicles at hippocampal synapses. Neuron *16*, 1197–1207.

Ryan, T.A., and Smith, S.J. (1995). Vesicle pool mobilization during action potential firing at hippocampal synapses. Neuron *14*, 983–989.

Smith, C., Moser, T., Xu, T., and Neher, E. (1998). Cytosolic Ca^{2+} acts by two separate pathways to modulated the supply of release-competent vesicles in chromaffin cells. Neuron *20*, 1243–1253.

Stevens, C.F., and Wesseling, J.F. (1998). Activity-dependent modulation of the rate at which synaptic vesicles become available to undergo exocytosis. Neuron *21*, 415–424.

Stewart, B.A., Atwood, H.L., Renger, J.J., Wang, J., and Wu, C.-F. (1994). Improved stability of *Drosophila* larval neuromuscular preparations in haemolymph-like physiological solutions. J. Comp. Physiol. A *175*, 179–191.

Zhong, Y., and Wu, C.-F. (1991). Altered synaptic plasticity in *Drosophila* memory mutants with a defective cAMP cascade. Science *251*, 198–201.

Zimmermann, H., and Whittaker, V.P. (1977). Morphological and biochemical heterogeneity of cholinergic synapses of the *Torpedo* electric organ. Neurosci. *2*, 715–730.

Zucker, R.S. (1996). Exocytosis: a molecular and physiological perspective. Neuron *17*, 1049–1055.